Journal of Computational and Applied Mathematics 379 (2020) 112947

Contents lists available at ScienceDirect

Journal of Computational and Applied Mathematics

journal homepage: www.elsevier.com/locate/cam

Finite element application of ERBS extraction

Tatiana Kravetc *, Rune Dalmo

R&D group Simulations, Department of Computer Science and Computational Engineering, Faculty of Engineering Science and Technology, UiT – The Arctic University of Norway, Norway

ARTICLE INFO

Article history:
Received 2 July 2019
Received in revised form 14 April 2020

Keywords:
Isogeometric analysis
Local projection
Extraction operator
Expo-rational basis functions

ABSTRACT

In this paper we explore ERBS extraction in application to a heat conduction problem. Two types of basis functions are considered: B-spline and expo-rational B-spline (ERBS) combined with Bernstein polynomials. The first one is a global basis defined on a subdomain whose size is related to the spline degree, while the second one is a strictly local basis under the local geometry. While all the coefficients of the B-spline tensor product surface affect each element of the patch, local surfaces of the blending surface conserve both local manipulation and smoothness of the global surface.

We show the conversion between these bases by using an ERBS extraction. The extraction operator allows us to convert the control points of the surface evaluated by B-splines to control points of the ERBS surface and vice versa. This approach is demonstrated on an example of the finite element solution approximation of the heat equation.

1. Introduction

In the isogeometric framework the solution space for dependent variables is represented in terms of the same functions which represent the geometry [1]. By utilizing the B-spline basis and its modifications, the standard finite element method based on the piecewise linear basis can be modified for the purpose of matching the exact geometry independently of the discretization. Weighted extended B-splines [2] were introduced as an alternative to standard mesh-based finite elements. However, in the context of isogeometric analysis, structures that precisely approximate the boundary are demanded. For this purpose, B-spline based tensor product [3] and triangular surfaces are used [4]. In addition, B-splines possess powerful tools for adaptive mesh refinement [5].

Investigations using tensor product NURBS constructions [6], T-spline constructions [7] and their Bézier and Lagrange extraction have shown that the use of a smooth basis in analysis provides computational advantages over standard finite elements in several areas. For instance, Bézier extraction has been used for efficient computations on volumes [8].

Expo-rational B-splines were introduced and explored in 2006 [9,10]. The expo-rational basis is strictly local and is used as a basis for blending local geometry. Thus, the ERBS tensor product surface is a blending of a set of local surfaces. The local geometry allows us to manipulate the blending surface independently, to perform efficient computations over a specific area and to avoid recomputation of the global problem unless necessary. In the isogeometric context, ERBS finite elements based on Taylor polynomials as local functions were applied in [11–13] to both rectangular and triangular elements. Besides ERBS, an alternative non-rational model for constructing free form curves and surfaces exists, namely, algebraic hyperbolic trigonometric (AHT) Bézier curves [14].

* Corresponding author.
E-mail address: tatiana.kravetc@uit.no (T. Kravetc).

https://doi.org/10.1016/j.cam.2020.112947

In this paper we propose to extract the linear operator which maps the expo-rational blending basis combined with the Bernstein polynomial basis of the local Bézier surfaces to the global B-spline basis. The transpose of the extraction operator maps the control points of the B-spline to the control points of the blending surface and vice versa.

We demonstrate some features of the extraction operator when applied to an example of a time-dependent heat conduction problem. We provide the conversion of the solution from a B-spline surface to an ERBS surface construction and vice versa, and compare them with an exact solution.

This paper is organized as follows. Section 2 focuses on the basic theory of B-splines, ERBS and a heat conduction problem, which is relevant for the proposed work. In Section 3 we define an extraction operator and describe its features. Section 4 and Section 5 provide the results and comparisons. Finally, we make some conclusions in Section 6.

2. Preliminaries

In this section we consider the definitions of B-spline and ERBS tensor product surfaces. The basic algorithm for solving a time-dependent heat conduction problem in the isogeometric framework is also described.

2.1. B-splines

One classical use of B-spline curves and surfaces is in the context of geometric modeling for the CAD industry.

For the knot vector $\{u_i\}_{i=0}^{n_u+p} = \{u_0, u_1, \ldots, u_n, u_{n+1}..., u_{n_u+p}\}$, where the first and the last $p+1$ knots are equal (i.e., $u_0 = u_1 = \cdots = u_p$ and $u_{n_u} = u_{n_u+1} = \cdots = u_{n_u+p}$), the B-spline basis functions are defined recursively [15] starting with a piecewise constant ($p = 0$)

$$N_{i,0}(u) = \begin{cases} 1, & \text{if } u_i \le u < u_{i+1}, \\ 0, & \text{otherwise.} \end{cases}$$

For $p = 1, 2, 3, \ldots$, they are defined by

A set $\mathbf{N}(u) = \{N_{i,p}\}_{i=0}^{n_u}$ forms a univariate B-spline basis of degree p. The simplest possibility of obtaining the bivariate B-spline basis is to form tensor product of univariate B-splines [2,16].

Let $\Theta = [0, 1] \times [0, 1]$ be a parametric domain with two independent parameters u and v, and $\mathbf{N}(u) = \{N_{i,p}\}_{i=0}^{n_u}$, $\mathbf{N}(v) = \{N_{j,p}\}_{j=0}^{n_v}$ be two row vectors of B-spline basis functions, defined on the corresponding knot vectors $\{u_i\}_{i=0}^{n_u+p}$ and $\{v_j\}_{j=0}^{n_v+p}$, where p is the spline degree. The bivariate B-spline basis functions is defined as

$$N_i(u, v) = N_{i,p}(u)\, N_{j,p}(v). \tag{1}$$

In the sequel of this paper any basis is represented as a row vector. For instance, a row vector of bivariate B-spline basis functions reads $\mathbf{N} = \mathbf{N}(u, v) = \{N_{\hat{i}}(u, v)\}_{\hat{i}=0}^{n_u n_v}$. An index $\hat{i}$ is expressed by sequential iteration over the indices i and j. Thus, the corresponding tensor product B-spline surface can be represented as an inner product of two vectors

$$S(u, v) = \mathbf{N}(u, v)\, \mathbf{P}, \tag{2}$$

where $\mathbf{P} \subset \mathbb{R}^3$ is a column vector of control points. Each control point corresponds to the appropriate basis function in the row vector $\mathbf{N}$.

The support of each B-spline basis function $N_{\hat{i}}(u, v)$ is compact and contained in the subdomain $[u_i, u_{i+p+1}] \times [v_j, v_{j+p+1}]$. Fig. 1(a) shows an example of one bivariate B-spline basis function defined on the parametric domain.

2.2. Expo-rational B-splines

We now consider some of the theory of blending type spline constructions, which is relevant for this work. A comprehensive study of the expo-rational B-splines (ERBS) can be found in [9,10].

Let $u = [0, 1]$ be a parameter subdivided into m_u intervals. An open knot vector defined on u has two multiple knots on both sides. The knots are numerated from 0 to $m_u + 2$. The simple version of an expo-rational basis function associated with the strictly increasing knots u_{k-1}, u_k and u_{k+1}, $k = 1, \ldots, m_u + 1$, is defined in [10] as

$$B_k(u) = \begin{cases} \Gamma_{k-1} \displaystyle\int_{u_{k-1}}^{u} \phi_{k-1}(s)ds, & \text{if } u_{k-1} < u \le u_k, \\ \Gamma_k \displaystyle\int_{u}^{u_{k+1}} \phi_k(s)ds, & \text{if } u_k < u < u_{k+1}, \\ 0, & \text{otherwise} \end{cases}$$

where

$$\phi_k(u) = \exp\left(-\frac{\left(u - \dfrac{u_k + u_{k+1}}{2}\right)^2}{(u - u_k)(u_{k+1} - u)} \right),$$

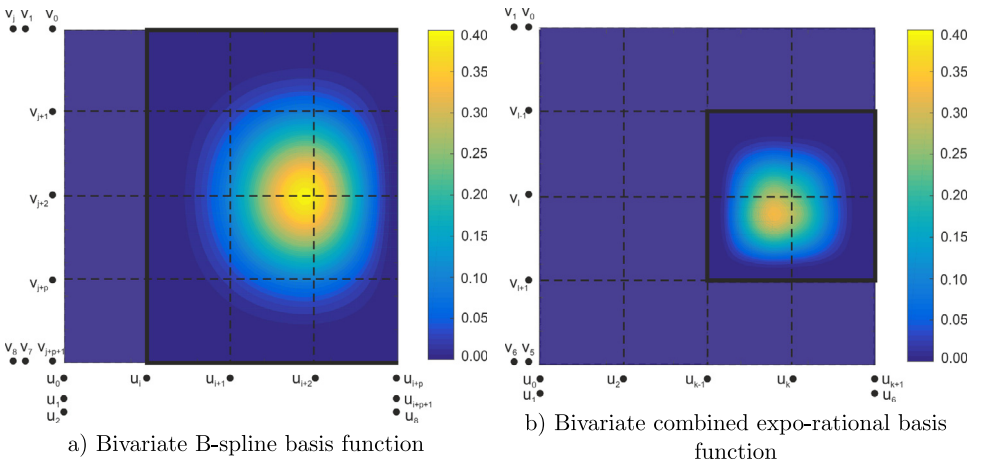

a) Bivariate B-spline basis function

b) Bivariate combined expo-rational basis function

Fig. 1. Comparison of contour plots of the B-spline and the combined expo-rational basis functions defined on the parametric domain Θ, subdivided into 4×4 elements. A contour plot of (a) one B-spline function $N_{\hat{\imath}}(u, v)$, $\hat{\imath} = (i, j)$, of degree $p = 3$ and (b) one combined expo-rational basis function $G_{\bar{\hat{k}}}(u, v)$, $\bar{\hat{k}} = (\bar{k}, \bar{l})$, of local degree $d = 1$ are shown. Bold lines frame subdomains where considered basis functions are nonzero.

and the scaling factor

$$\Gamma_k = \frac{1}{\int_{u_k}^{u_{k+1}} \phi_k(u) du}.$$

An expo-rational B-spline curve is described by

$$A(u) = \sum_{k=1}^{m_u+1} B_k(u) \ell_k, \tag{3}$$

where ℓ_k, $k = 1, \ldots, m_u + 1$ are the respective local functions, which are Bézier curves in our case. Each Bézier curve is defined as a linear combination of control points and Bernstein polynomials. Moreover, they are scaled and translated to the interval $[u_{k-1}, u_{k+1}]$. For this, we introduce a local/global mapping $\omega_k(u)$, which scales the support of the local curves ℓ_k to the interval $[u_{k-1}, u_{k+1}]$.

$$\omega_k(u) = \begin{cases} \dfrac{u - u_{k-1}}{u_{k+1} - u_{k-1}}, & u_{k-1} < u \leq u_{k+1}, \\ 0, \quad \text{otherwise.} \end{cases}$$

Thus, the local Bézier curve ℓ_k, $k = 1, \ldots, m_u + 1$ is defined as

$$\ell_k = \sum_{a=0}^{d} b_{d,a}(\omega_k(u))\, q_{k,a}, \tag{4}$$

where $q_{k,a}$ are the control points of the kth local curve, and $b_{d,a}$ are the Bernstein polynomials of degree d, which are generated by the general formula

$$b_{d,a}(t) = \binom{d}{a} t^a (1-t)^{d-a} = \frac{d!}{a!(d-a)!} t^a (1-t)^{d-a}.$$

By combining (4) and (3) the ERBS curve can be represented as

To be able to apply the FEM approach to blending splines, we separate control points from basis functions. Thus, we merge Bernstein polynomials and expo-rational basis, and introduce *the combined expo-rational basis*

$$G_{\bar{k}}(u) = b_{d,a}(\omega_k(u))\, B_k, \quad k = 1, \ldots, m_u + 1, \;\; a = 0, \ldots, d, \tag{5}$$

where the index $\bar{k}$ numerates the local basis function with respect to the global knot index k and the local iterator a.

A similar approach to the basis restructuring was considered for the one dimensional case in [17], where it was compared to polynomial basis.

We proceed by assembling a row vector of univariate combined expo-rational basis functions $\mathbf{G}(u) = \{G_{\bar{k}}(u)\}_{\bar{k}=1}^{(m_u+1)(d+1)}$. The combined expo-rational basis possesses the following properties:

- the basis functions constitute a partition of unity;
- linear independence;
- minimal support of the basis functions;
- transfinite Hermite interpolation property.

The expo-rational tensor product surface resembles the usual B-spline tensor product surface, except that coefficients are not points, but surfaces, which are blended locally by using expo-rational basis functions.

Employing the approach of forming a bivariate basis, described similarly for the B-spline basis above, recall (1), we obtain the bivariate combined expo-rational basis function with index $\hat{\bar{k}}$ as

$$G_{\hat{\bar{k}}}(u, v) = G_{\bar{k}}(u)\, G_{\bar{l}}(v),$$

where $\{G_{\bar{k}}(u)\}_{\bar{k}=1}^{(m_u+1)(d+1)}$ and $\{G_{\bar{l}}(v)\}_{\bar{l}=1}^{(m_v+1)(d+1)}$ form two row vectors of univariate combined expo-rational bases $\mathbf{G}(u)$ and $\mathbf{G}(v)$, respectively, in accordance with formula (5), defined on the corresponding knot vectors $\{u_k\}_{k=0}^{m_u+2}$ and $\{v_l\}_{l=0}^{m_v+2}$. These vectors form a mesh on the parametric domain Θ, i.e. the knot intervals subdivide the domain into finite elements.

A blending tensor product surface is defined as

$$A(u, v) = \mathbf{G}(u, v)\,\mathbf{Q}, \tag{6}$$

where $\mathbf{Q} \subset \mathbb{R}^3$ is a column vector of control points, composing a set of local Bézier surfaces, and $\mathbf{G} = \mathbf{G}(u, v) = \{G_{\hat{\bar{k}}}(u, v)\}_{\hat{\bar{k}}=1}^{(m_u+1)(m_v+1)(d+1)^2}$ is a row vector of bivariate combined expo-rational basis functions. The index $\hat{\bar{k}}$ iterates over the indices $\bar{k}$ and $\bar{l}$ in such a way that the sets $\mathbf{G}$ and $\mathbf{Q}$ are consequent.

The locality of the bivariate B-spline basis function and the combined expo-rational basis function are compared in Fig. 1. One can see that the support of each combined expo-rational basis function (Fig. 1(b)) is contained within the subdomain $[u_{k-1}, u_{k+1}] \times [v_{l-1}, v_{l+1}]$, while each B-spline basis function (Fig. 1(a)) is defined on the patch of size $p+1 \times p+1$. One of the features of blending type surfaces is that the combined expo-rational basis functions are nonzero only under the local geometry cover. Specific locality gives them an advantage also over C^0 nodal bases, since the overlapping of local surfaces preserves smoothness between nodes.

2.3. Model problem

In this section we consider time-dependent heat conduction [18] as an illustrative model problem.

$$\frac{\partial T}{\partial \tau} - \Delta T = f, \qquad \text{in } \Omega,\ \tau > 0, \tag{7}$$

$$\text{BC:} \qquad -\frac{\partial T}{\partial n} = \kappa(T - T_D) - T_N, \quad \text{on } \partial\Omega,\ \tau \geq 0, \tag{8}$$

$$\text{IC:} \qquad T(\Omega, 0) = T_0, \qquad \text{in } \Omega, \tag{9}$$

where Δ is the Laplace operator, Ω is a bounded convex domain with boundary $\partial\Omega$, $\tau > 0$ time, T is the temperature to determine, $f(x, y, \tau)$ is a given source function. Boundary conditions (8) are the Robin boundary conditions, where $\frac{\partial}{\partial n}$ is differentiation in the outward normal direction to $\partial\Omega$, κ is a constant for determining the Dirichlet or Neumann type of the boundary conditions, T_D and T_N are given functions. An initial condition (9) is given as $T_0(x, y)$, and (x, y) are Cartesian coordinates.

Let Υ be a set of test functions, such that $\Upsilon = \{\upsilon \in H^1(\Omega) : \upsilon = 0 \text{ on } \partial\Omega\}$. The variational formulation reads: find the solution $T \in H^1(\Omega)$ that satisfies the boundary conditions and

$$\int_\Omega \dot{T}\upsilon\, dxdy + \int_\Omega \nabla T\, \nabla\upsilon\, dxdy + \int_{\partial\Omega} \kappa\, T\upsilon\, ds = \\ = \int_\Omega f\upsilon\, dxdy + \int_{\partial\Omega} (\kappa\, T_D + T_N)\upsilon\, ds, \quad \forall\, \upsilon \in \Upsilon. \tag{10}$$

For simplicity, we opt for a square domain $\Omega = [0, 1]\times[0, 1]$ and Dirichlet boundary conditions $T = T_D$ on $\partial\Omega$. In order to discretize the variational formulation in space, we represent a real domain Ω as a parametric domain $\Theta = [0, 1]\times[0, 1]$ with two independent parameters (u, v) and introduce a mesh with m elements. The discretized temperature field is represented as

$$T_h(\Theta, \tau) = \mathbf{H}\,\zeta(\tau), \tag{11}$$

where $\zeta(\tau)$ is a column vector of time-dependent coefficients and $\mathbf{H}$ is a row vector of bivariate basis functions defined on the parametric domain Θ.

Substituting (11) into the variational formulation (10) and replacing the test functions υ with the basis functions $\mathbf{H}$, we obtain a variational formulation discretized in space.

To discretize the problem in time, let $0 = \tau_0 < \tau_1 < \cdots \leq \tau_L$ be a time grid with the time steps $\Delta\tau_l = \tau_l - \tau_{l-1}$, $l = 1, 2, \ldots, L$. Then the solution T_h can be expressed for every fixed time step. This approximation of the solution is fully discrete in the sense that it is only defined for the discrete times τ_l.

After the discretization in both space and time we obtain the following matrix equation

$$(\mathcal{M} + \Delta\tau_l(\mathcal{A} + \mathcal{R}))\zeta_l = \mathcal{M}\zeta_{l-1} + \Delta\tau_l(b + r), \tag{12}$$

where ζ_l denotes a vector of time-dependent coefficients at time τ_l, mass matrix $\mathcal{M}$, stiffness matrix $\mathcal{A}$ and source vector b are defined as

$$\mathcal{M} = \int_{\Theta} \mathbf{H}^{\mathrm{T}}\mathbf{H}\, dudv, \quad \mathcal{A} = \int_{\Theta} \nabla\mathbf{H}^{\mathrm{T}}\nabla\mathbf{H}\, dudv, \quad b = \int_{\Theta} f(\tau_l)\,\mathbf{H}^{\mathrm{T}}\, dudv,$$

boundary matrix $\mathcal{R}$ and boundary vector r are defined as

$$\mathcal{R} = \int_{\partial\Theta} \kappa\,\mathbf{H}^{\mathrm{T}}\mathbf{H}\, dw, \quad r = \int_{\partial\Theta} \kappa\, T_D\,\mathbf{H}^{\mathrm{T}}\, dw.$$

An initial condition T_0 (9) can be approximated by using the L^2-projection, i.e. by solving the matrix equation

$$\int_{\Theta} \mathbf{H}^{\mathrm{T}}\mathbf{H}\, dudv\, \zeta_0 = \int_{\Theta} T_0\,\mathbf{H}^{\mathrm{T}}\, dudv,$$

which gives us a set of initial coefficients ζ_0. Thus, the initial condition is derived as

$$T_h(\Theta, 0) = \mathbf{H}\,\zeta_0.$$

3. Extraction operator

In this section, we describe the decomposition of the combined expo-rational basis into the B-spline basis. Detailed studies of computing the extraction operator can be found in [6,7,19].

The expo-rational extraction for B-splines determines the representation of the B-spline basis over each element in terms of a set of expo-rational basis functions. The extraction operation is based on basis decomposition and follows from the linear independence of the bases. The purpose of the presented work is to convert the global B-spline representation to a local smooth representation. This conversion is obtained in a discrete way, which yields a relative inaccuracy, since we convert polynomials into non-polynomial and strictly local functions. However, the accuracy can be controlled via adjusting the number of evaluating points.

To provide an extraction between two bases, we need to notice that the number of B-spline basis functions should be equivalent to the number of expo-rational combined basis functions *locally*, i.e., on each element. This restriction can be met by the relation

$$(p + 1) \equiv 2(d + 1), \tag{13}$$

where p is the B-spline degree, and d is the degree of the local Bézier surfaces of the blending surface construction.

We focus on a single element Θ^e, $e = 1, \ldots, m$, of the parametric domain. Let us introduce two new parameters $\xi \in [0, 1]$ and $\eta \in [0, 1]$ for this element. Since both the B-spline and the combined expo-rational basis functions are linearly independent, and supposing that the restriction (13) is fulfilled, we can represent the B-spline basis as a linear combination of the combined expo-rational basis functions.

Let $N_\iota^e(\xi, \eta)$, with index $\iota = 1, \ldots, (p + 1)^2$ and degree p, be a set of localized B-spline basis functions, i.e., the parts of the bivariate B-spline basis functions defined over the element Θ^e only. Similarly, we define a localized set of the combined expo-rational basis functions $G_\delta^e(\xi, \eta)$, $\delta = 1, \ldots, 4(d + 1)^2$. An example of both these sets is shown in Fig. 2. From the linear independency of both these sets and restriction (13) it follows that over the element Θ^e for a localized B-spline function $N_\iota^e(\xi, \eta)$ there exist coefficients $\epsilon_{\iota,\delta}^e$ such that

$$N_\iota^e(\xi, \eta) = \sum_{\delta=1}^{4(d+1)^2} \epsilon_{\iota,\delta}^e\, G_\delta^e(\xi, \eta). \tag{14}$$

Bearing in mind that in this paper we represent a set of basis functions as the row vector, one can write formula (14) in matrix form as

$$(\mathbf{N}^e(\xi, \eta))^{\mathrm{T}} = \mathbf{E}^e\,(\mathbf{G}^e(\xi, \eta))^{\mathrm{T}}. \tag{15}$$

The matrix $\mathbf{E}^e$ is called *the element extraction operator*. It maps one basis to another over the element. The reverse conversion can be obtained by the formula

Fig. 2 illustrates the bases, defined on the element Θ^e, which can be converted one to another and vice versa by using the extraction operator $\mathbf{E}^e$.

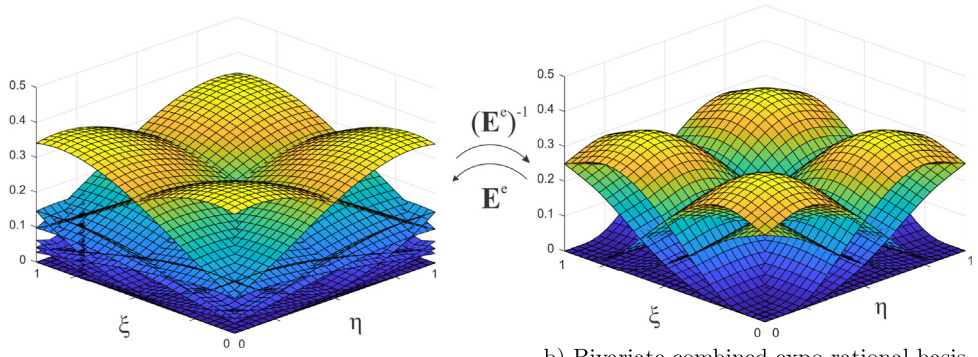

a) Bivariate B-spline basis functions $N^e_\iota(\xi,\eta)$, $\iota = 1,...,(p+1)^2$, on the element Θ^e

b) Bivariate combined expo-rational basis functions $G^e_\delta(\xi,\eta)$, $\delta = 1,...,4(d+1)^2$, on the element Θ^e

Fig. 2. An extraction operator $\mathbf{E}^e$ converts the bivariate B-spline to expo-rational basis functions and vice versa on an element level.

The conversion between B-spline and expo-rational tensor product surfaces is performed locally, i.e. on each element Θ^e. This means that, in accordance with the number of localized basis functions, we get the same number of control points over each element, independently of the type of conversion: from B-spline to blending surface or vice versa.

Let $\mathbf{P}^e$ be a column vector of control points formed an element $S^e(\xi,\eta)$ of the B-spline tensor product surface, and $\mathbf{Q}^e$ be a column vector of control points for four local surfaces, whose blending gives an element $A^e(\xi,\eta)$ of the expo-rational tensor product surface. By considering an element level, and substituting (15) into (2), we represent the B-spline surface (2) in terms of the expo-rational blending surface (6) as follows

$$S^e(\xi,\eta) = \mathbf{N}^e(\xi,\eta)\mathbf{P}^e = \mathbf{G}^e(\xi,\eta)(\mathbf{E}^e)^{\mathrm{T}}\mathbf{P}^e = \mathbf{G}^e(\xi,\eta)\mathbf{Q}^e = A^e(\xi,\eta). \tag{16}$$

From (16) we conclude that the control points of both locally evaluated surfaces can be converted as $\mathbf{Q}^e = (\mathbf{E}^e)^{\mathrm{T}}\mathbf{P}^e$ and $\mathbf{P}^e = (\mathbf{E}^e)^{-\mathrm{T}}\mathbf{Q}^e$ since the extraction operator is invertible.

An element-level conversion from a B-spline control net to an expo-rational tensor product surface $A^e(\xi,\eta)$ can be obtained by the following formula: for each element Θ^e, $e = 1,\ldots,m$,

$$A^e(\xi,\eta) = \mathbf{G}^e(\xi,\eta)(\mathbf{E}^e)^{\mathrm{T}}\mathbf{P}^e. \tag{17}$$

The inverse conversion can then be formulated as

$$S^e(\xi,\eta) = \mathbf{N}^e(\xi,\eta)(\mathbf{E}^e)^{-\mathrm{T}}\mathbf{Q}^e. \tag{18}$$

The conversions (17) and (18) are illustrated in Fig. 3 for a fifth degree B-spline and a blending tensor product surface with local Bézier surfaces of degree 2. On the left hand side one can see the B-spline control net consisting of 6×6 points and the corresponding element of the tensor product surface. On the right hand side a similar surface element is represented as the blending of local geometry utilizing the expo-rational basis (note that only two of four local surfaces are shown). For such a local representation the number of control points for both kinds of surfaces is equivalent, which allows for conversion between the two representations.

4. Numerical experiments

In this section we compare two types of bases and conversion between appropriate solutions. Several mesh types are used for the illustration. Fig. 4 shows some examples of the mesh configurations, corresponding control nets for the B-spline surface and local surfaces of the blending type tensor product surface. In accordance with the restriction (13), the B-spline and ERBS representation of the surface are consistent, i.e. convertible one to another, for each row (1)-(3) in Fig. 4. Note that the local surfaces illustrated in Fig. 4(c) are scaled to be easier recognizable. In reality, they partially overlap neighbor local surfaces. The support of each local surface covers four neighbor elements.

In order to compare performance of the conversion method, we consider two heat conduction problems. The one is a time-dependent equation (7)–(9) with homogeneous Dirichlet boundary conditions, whose initial condition is not smooth, while its steady-state solution is smooth. Let us consider two states of the system ($\tau = 0$ and $\tau = \infty$) as two illustrative examples, which demonstrate some possibilities of the ERBS extraction operator in the FEM context. In addition, the time-dependent simulation of the approximated solution using B-spline, ERBS tensor product surfaces and their conversions one to another illustrates the variate precision of the different approaches.

We specify given functions in the model problem (7)–(9) as follows

$$f = -2xy(x^2 + y^2 - 2),$$

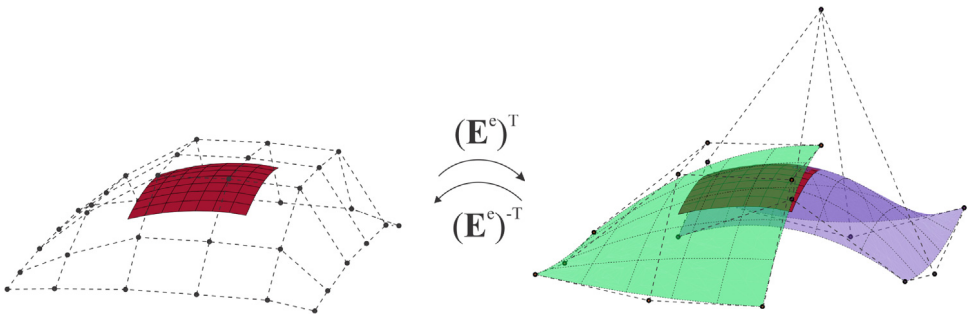

Fig. 3. The transpose of the extraction operator converts the local B-spline control points to control points of local surfaces of the expo-rational tensor product surface and vice versa on an element level.

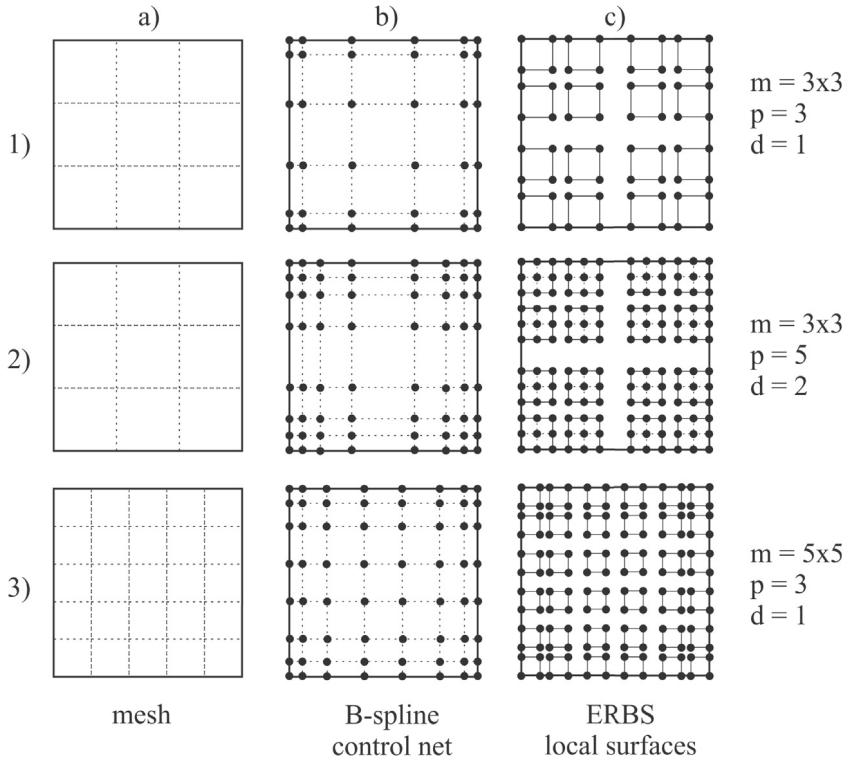

Fig. 4. Examples of some mesh configurations. The columns (b) and (c) demonstrate correspondence between the B-spline (degree p) control net and the set of local surfaces (degree d) of blending tensor product surface.

$$T_D = T_N = 0, \quad \kappa = 10^6, \quad \Omega = [0,1] \times [0,1],$$

$$T_0 = (0.5 - |0.5 - x|)(0.5 - |0.5 - y|). \tag{19}$$

An exact steady-state solution for this problem is

$$T(\Omega, \infty) = \frac{1}{3}(x^3 - x)(y^3 - y). \tag{20}$$

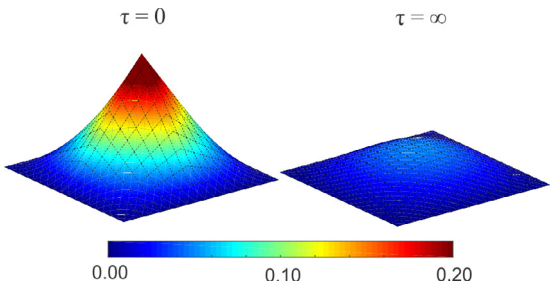

Fig. 5. An exact solution of the heat conduction problem. An initial condition ($\tau = 0$) and a steady-state solution ($\tau = \infty$) are shown.

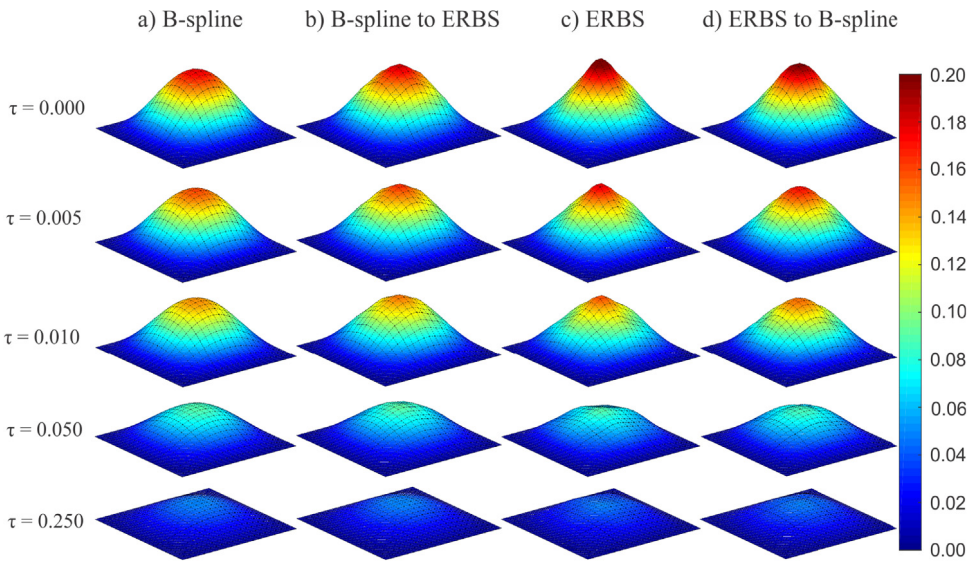

Fig. 6. Time-dependent simulation of the time-dependent heat conduction problem. (a) and (c) are two different simulations formed by the B-spline and the combined expo-rational basis, respectively. (b) and (d) are the corresponding conversions of the time-dependent solutions.

We compare finite element approaches based on the B-spline basis, the combined expo-rational basis, and the conversions between corresponding coefficients of the approximated surface (see Fig. 3) with exact solutions for $\tau = 0$ and $\tau = \infty$. The corresponding exact solutions (19) and (20) are shown in Fig. 5.

The second problem is a steady-state heat equation $-\Delta T = f$ with inhomogeneous Dirichlet boundary conditions. The given functions are specified as

$$f = 0, \quad \Omega = [0, 1] \times [0, 1],$$

$$T(0, y) = T(1, y) = 0, \qquad T(x, 0) = -1, \qquad T(x, 1) = 1.$$

An exact solution for this problem is

$$T(\Omega) = \frac{2}{\pi} \sum_{n=1}^{\infty} \frac{(-1)^{n+1} + 1}{n} \frac{\sinh(n\pi(y - 1/2))}{\sinh(n\pi/2)} \sin(n\pi x). \tag{21}$$

Fig. 7 shows the boundary conditions and the exact solution (21) of the second problem.

The problems described above are solved by using both the B-spline basis and the combined expo-rational basis. These solutions are shown in Figs. 6, 8, respectively. An original approximation of the solution, shown in Figs. 6(a), (c) and 8(a), (c), is obtained by solving the matrix equation (12), where the basis **H** is replaced with the B-spline basis **N** and the combined expo-rational basis **G**, respectively. The conversion from control points of the B-spline surface to control points of the local geometry of the expo-rational tensor product surface, shown in Figs. 6(b) and 8(b), is obtained by formula (17). The conversion from ERBS surface to B-spline surface, shown in Figs. 6(d) and 8(d), is obtained by formula (18). The mesh configuration shown in Fig. 4(1) is used.

A coarse mesh of size 3×3 was selected to better illustrate the different approaches. From the locality of the combined expo-rational basis it follows that we obtain improved approximation of non-smooth surfaces when compared to the

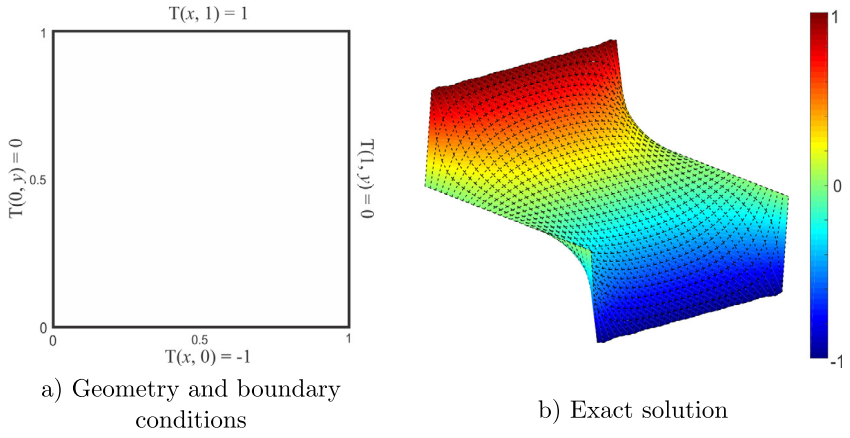

Fig. 7. An example of the heat conduction problem with inhomogeneous Dirichlet boundary conditions.

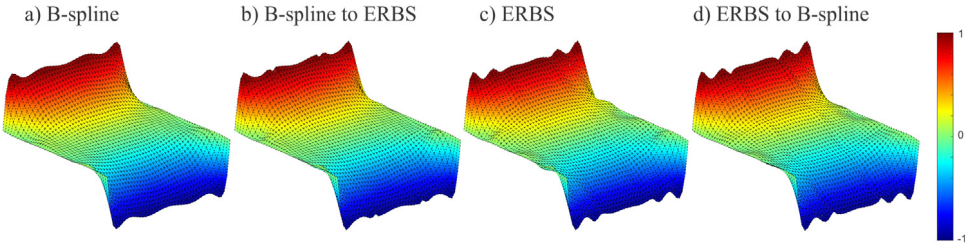

Fig. 8. Simulation of the heat conduction problem with inhomogeneous Dirichlet boundary conditions. (a) and (c) are two different simulations formed by the B-spline and the combined expo-rational basis, respectively. (b) and (d) are the corresponding conversions of the solution.

B-spline of low degree ($p = 3$) on the uniform domain, as shown in Fig. 6, $\tau = 0$. A smooth steady-state solution is approximated better by the B-spline tensor product surface than by the blending spline tensor product surface with first degree of local surfaces, which is demonstrated in Fig. 9(1b), (3b).

For the problem with inhomogeneous Dirichlet boundary conditions, shown in Fig. 8, a shape of the solution surface leads to some oscillation in its approximation due to discontinuity of the boundary conditions. Here the B-spline of bi-degree $(p_u, p_v) = (7, 3)$ and the combined expo-rational basis of local bi-degree $(d_u, d_v) = (3, 1)$ are used for the approximation. Therefore, we obtain a more accurate approximation along the parameter u.

5. Summary of the results

Three illustrative examples are generated in Section sec:numtests. In this section we compare their performance. *Example 1* and *Example 2* are based on the time-dependent heat equation (see Fig. 6). *Example 1*, shown in Fig. 6, $\tau = 0$, is an approximation of the initial condition while *Example 2*, shown in Fig. 6, $\tau = 0.25$, is an approximation of the steady-state solution. *Example 3*, shown in Fig. 8, is an approximated solution of the heat equation with inhomogeneous Dirichlet boundary conditions.

Fig. 9 compares absolute errors for each example on the mesh configuration shown in Fig. 4(3). The B-spline degree $p = 3$, the local degree of ERBS surface $d = 1$ for the examples 1 and 2. In the third example $(p_u, p_v) = (7, 3)$, $(d_u, d_v) = (3, 1)$. The error scaling is selected differently for each example due to different maximum error. Converted surfaces are evaluated at the element level, which is reflected in the error plots. An ERBS surface obtained from B-spline approximation of the steady-state solution (Fig. 9(2b)) has a smaller error than the original ERBS approximation (Fig. 9(3b)). A B-spline conversion from the ERBS approximation of the initial condition (Fig. 9(4a)) demonstrates improved performance over the original B-spline approximation (Fig. 9(1a)). The reason for this is the locality of the conversion scheme, i.e., the control points of the blending surface in each element are directly mapped to control points of a suitable B-spline patch. A similar effect can be observed in Fig. 8(b), where the resulting converted surface has some inconsistency between elements due to the locality of the conversion scheme. The third example, shown in Fig. 9(c), demonstrates that the conversion scheme provides almost identical surfaces when the mesh is denser and the spline degree is relatively high.

Different types of errors for the proposed examples and mesh configurations are listed in Tables 1–3. Two types of basis functions: B-spline and combined expo-rational are presented. For each combination of mesh size, spline type and

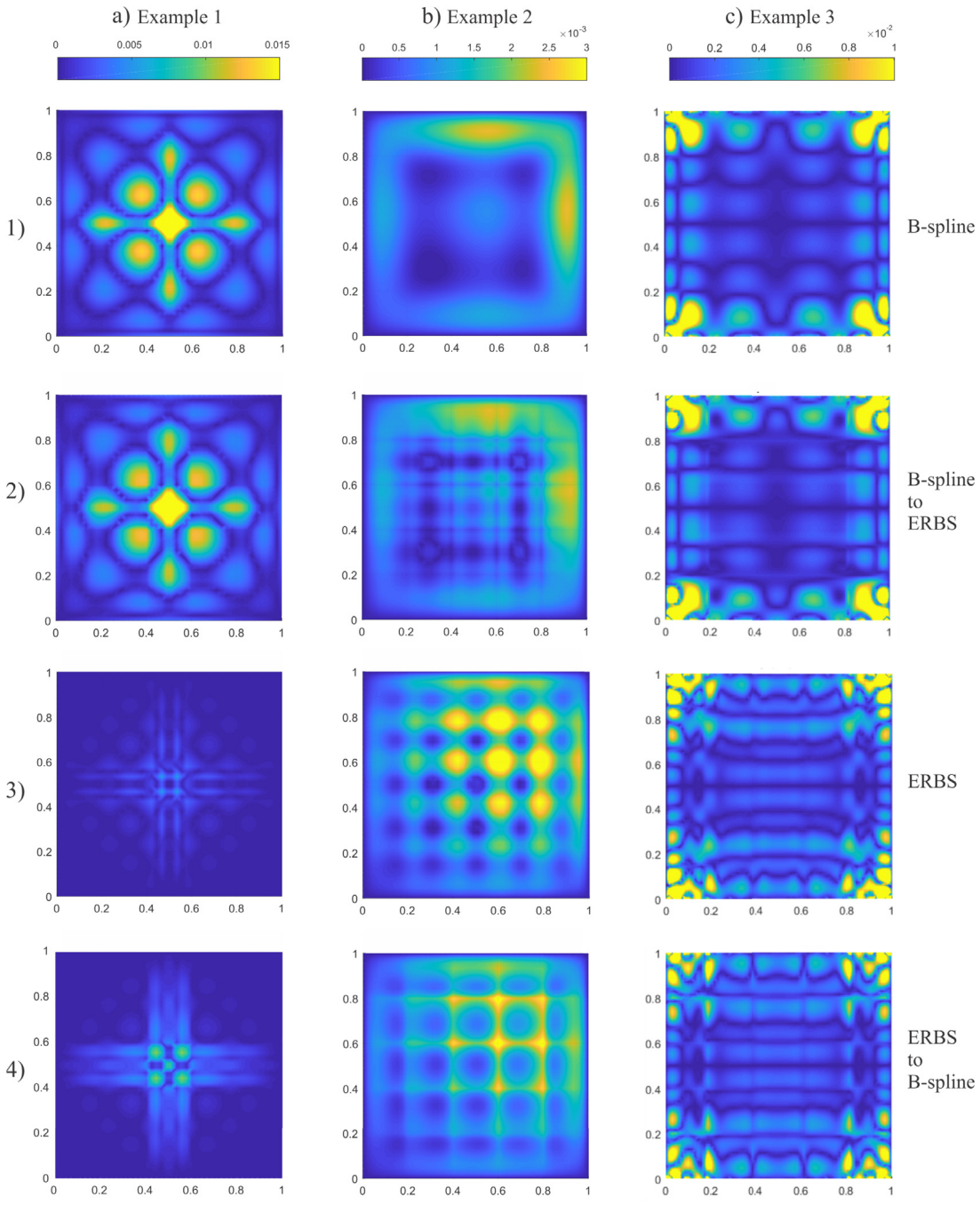

Fig. 9. Comparison of absolute errors for B-spline and combined expo-rational bases, conversion from B-spline surface to blending surface and vice versa. A mesh of size 5×5 is used.

its degree, the corresponding conversions are provided: B-spline control points to local surfaces, and local surfaces to B-spline control points.

One can see that increasing of both spline degree and number of elements reduces the difference between an original approximation (B-spline or ERBS) and its conversion to another one. In general, the accuracy of the conversion depends on the shape of the approximated surface. For instance, an ERBS approximation of a non-smooth surface, see Table 1, is better than the B-spline due to the strict locality of the expo-rational basis. Thus, the blending spline representation of B-spline (B-spline to ERBS) is more accurate than ERBS to B-spline.

An approximation of a smooth surface, see Table 2, provides comparable results for both B-spline and ERBS cases.

Table 1
Comparison of different types of errors for the first example, i.e. approximation of the initial condition (19) obtained by L^2 projection.

Example 1					
Mesh size	Degree	Basis	Max error	Average error	L^2 error
3×3	$p = 3$	B-spline	0.0418	5.85×10^{-3}	0.00702
		B-spline to ERBS	0.0351	5.41×10^{-3}	0.00661
	$d = 1$	ERBS	0.0083	7.90×10^{-4}	0.00101
		ERBS to B-spline	0.0157	1.81×10^{-3}	0.00254
	$p = 5$	B-spline	0.0259	3.50×10^{-3}	0.00387
		B-spline to ERBS	0.0259	3.41×10^{-3}	0.00386
	$d = 2$	ERBS	0.0076	5.53×10^{-4}	0.00085
		ERBS to B-spline	0.0081	7.10×10^{-4}	0.00108
5×5	$p = 3$	B-spline	0.0330	3.23×10^{-3}	0.00404
		B-spline to ERBS	0.0295	3.14×10^{-3}	0.00386
	$d = 1$	ERBS	0.0054	3.47×10^{-4}	0.00045
		ERBS to B-spline	0.0102	7.39×10^{-4}	0.00143
	$p = 5$	B-spline	0.0245	2.35×10^{-3}	0.00282
		B-spline to ERBS	0.0245	2.31×10^{-3}	0.00281
	$d = 2$	ERBS	0.0048	2.24×10^{-4}	0.00036
		ERBS to B-spline	0.0043	2.51×10^{-4}	0.00032

Table 2
Comparison of different types of errors for the second example, i.e. approximation of the steady-state solution (20) obtained by solving the time-dependent heat equation.

Example 2					
Mesh size	Degree	Basis	Max error	Average error	L^2 error
3×3	$p = 3$	B-spline	0.0040	1.46×10^{-3}	0.00188
		B-spline to ERBS	0.0046	1.67×10^{-3}	0.00207
	$d = 1$	ERBS	0.0067	2.10×10^{-3}	0.00263
		ERBS to B-spline	0.0067	1.83×10^{-3}	0.00224
	$p = 5$	B-spline	0.0033	9.13×10^{-4}	0.00119
		B-spline to ERBS	0.0033	8.99×10^{-4}	0.00117
	$d = 2$	ERBS	0.0032	1.26×10^{-3}	0.00151
		ERBS to B-spline	0.0040	1.27×10^{-3}	0.00154
5×5	$p = 3$	B-spline	0.0024	7.20×10^{-4}	0.00094
		B-spline to ERBS	0.0024	7.93×10^{-4}	0.00102
	$d = 1$	ERBS	0.0036	1.17×10^{-3}	0.00147
		ERBS to B-spline	0.0036	1.05×10^{-3}	0.00130
	$p = 5$	B-spline	0.0019	4.33×10^{-4}	0.00060
		B-spline to ERBS	0.0019	4.28×10^{-4}	0.00059
	$d = 2$	ERBS	0.0019	6.24×10^{-4}	0.00079
		ERBS to B-spline	0.0020	6.18×10^{-4}	0.00063

Since the solution in the third example oscillates, maximum error is relatively large, see Table 3. However, a smoothing property of the conversion scheme, which follows from the fact that an extraction operator does not provide exact mapping between B-spline and ERBS representations, reduces this oscillation on average. Various (p_u, p_v)-degrees, with $p_u \neq p_v$, can be successfully used in the conversion scheme where appropriate.

6. Conclusion

We have implemented and explored the global finite element method technique in the context of B-splines, and its conversion to a strictly local representation. These modifications were obtained by using an extraction operator which maps the combination of the expo-rational basis and the local Bernstein polynomial basis of the Bézier local surfaces to the global bivariate B-spline basis. The extraction operator localizes the topological and global smoothness information to the element level. The conversion between coefficients of the B-spline tensor product surface and expo-rational tensor product surface yields an approximation, which is very close to the B-spline, but strictly locally represented.

Standard triangular and rectangular finite elements can be obtained for C^0 continuity [20]. The B-spline basis of degree p is $(p - 1)$-times continuously differentiable with discontinuities of the pth derivative at the knot points [2]. As an

Table 3
Comparison of different types of errors for the third example, i.e. approximation of the solution (21) obtained by solving the steady-state heat equation with inhomogeneous Dirichlet boundary conditions.

Example 3					
Mesh size	Degree	Basis	Max error	Average error	L^2 error
3×3	$p = 5$	B-spline	0.4232	1.92×10^{-2}	0.04386
		B-spline to ERBS	0.4965	1.95×10^{-2}	0.04375
	$d = 2$	ERBS	0.4531	1.83×10^{-2}	0.03787
		ERBS to B-spline	0.4790	1.93×10^{-2}	0.04154
	$p = 7$	B-spline	0.3022	1.39×10^{-2}	0.03268
		B-spline to ERBS	0.3901	1.38×10^{-2}	0.03181
	$d = 3$	ERBS	0.3511	1.62×10^{-2}	0.03075
		ERBS to B-spline	0.3743	1.67×10^{-2}	0.03096
	$(p_u, p_v) =$	B-spline	0.3189	1.58×10^{-2}	0.03606
	$= (7, 3)$	B-spline to ERBS	0.4027	1.61×10^{-2}	0.03685
	$(d_u, d_v) =$	ERBS	0.3711	1.76×10^{-2}	0.03904
	$= (3, 1)$	ERBS to B-spline	0.3921	1.87×10^{-2}	0.03632
5×5	$p = 5$	B-spline	0.2418	1.19×10^{-2}	0.01360
		B-spline to ERBS	0.2975	1.19×10^{-2}	0.01214
	$d = 2$	ERBS	0.2707	1.04×10^{-2}	0.01405
		ERBS to B-spline	0.2693	1.07×10^{-2}	0.01063
	$p = 7$	B-spline	0.1000	8.63×10^{-3}	0.01044
		B-spline to ERBS	0.1322	8.62×10^{-3}	0.00926
	$d = 3$	ERBS	0.1096	9.58×10^{-3}	0.01047
		ERBS to B-spline	0.1155	9.76×10^{-3}	0.00930
	$(p_u, p_v) =$	B-spline	0.1725	1.11×10^{-2}	0.01228
	$= (7, 3)$	B-spline to ERBS	0.1455	1.09×10^{-2}	0.01199
	$(d_u, d_v) =$	ERBS	0.2035	1.07×10^{-2}	0.01265
	$= (3, 1)$	ERBS to B-spline	0.2212	1.05×10^{-2}	0.01059

alternative tool, ERBS basis functions provide C^∞ continuity between knots. The approximation order of the blending spline construction depends on the continuity of local polynomial functions [9]. Moreover, blending surfaces provide an additional level of abstraction. While coefficients of the standard finite element coincide with nodal points, and the coefficients of the B-spline tensor product surface affect each element of the corresponding basis support, the local surfaces of the blending type spline construction preserve both local representation and smoothness of the global surface.

The expo-rational basis, in contrast to a B-spline basis, possesses an interpolatory property, it is symmetric on each element, and it is represented as a local basis under the local geometry. It allows us to perform computations at the element level and to be more efficient, because the basis functions have identical shape independently on the element index (except at the boundary).

The proposed approach can be utilized in mesh refinement schemes. In accordance with the possibilities of moving and inserting knots to blending surface constructions [21], several types of mesh refinements can be considered for future investigation.

References

[1] T.J.R. Hughes, J.A. Cottrell, Y. Bazilevs, Isogeometric analysis: CAD, finite elements, NURBS, exact geometry and mesh refinement, Comput. Methods Appl. Mech. Engrg. 194 (2005) 4135–4195.
[2] K. Höllig, Finite Element Methods with B-splines, Society for Industrial and Applied Mathematics, Philadelphia, 2003.
[3] D. Schillinger, P.K. Ruthala, L.H. Nguyen, Lagrange Extraction and projection for NURBS basis functions: A direct link between isogeometric and standard nodal finite element formulations, Internat. J. Numer. Methods Engrg. 108 (2016) 515–534.
[4] Y. Jia, Y. Zhang, G. Xu, X. Zhuang, T. Rabczuk, Reproducing kernel triangular B-spline-based FEM for solving PDEs, Comput. Methods Appl. Mech. Engrg. 267 (2013) 342–358.
[5] G. Xu, B. Li, L. Shu, L. Chen, J. Xu, T. Khajah, Efficient r-adaptive isogeometric analysis with Winslow's mapping and monitor function approach, J. Comput. Appl. Math. 351 (2019) 186–197.
[6] M.J. Borden, M.A. Scott, J.A. Evans, T.R.J. Hughes, Isogeometric finite element data structures based on Bézier extraction of NURBS, Internat. J. Numer. Methods Engrg. 87 (2010) 15–47.
[7] M.J. Borden, M.A. Scott, C.V. Verhoosel, T.W. Sederberg, T.R.J. Hughes, Isogeometric finite element data structures based on Bézier extraction of T-splines, Internat. J. Numer. Methods Engrg. 00 (2010) 1–40.
[8] G. Xu, T.-H. Kwok, C.C.L. Wang, Isogeometric computation reuse method for complex objects with topology-consistent volumetric parameterization, Comput. Aided Des. 91 (2017) 1–13.
[9] L.T. Dechevsky, A. Laksså, B. Bang, Expo-rational B-splines, Int. J. Pure Appl. Math. 27 (3) (2006) 319–367.
[10] A. Laksså, Basic Properties of Expo-Rational B-Splines and Practical Use in Computer Aided Geometric Design (Ph.D. thesis), University of Oslo, 2007.

[11] P. Zanaty, Finite element methods based on a generalized expo-rational B-splines with harmonic polynomial coefficients, Int. J. Appl. Math. 26(3) (2013) 379–390.
[12] L.T. Dechevsky, P. Zanaty, First instances of univariate and tensor-product multivariate generalized expo-rational finite elements , in: Applications of Mathematics and Engineering and Economics 2011, 1410, American Institute of Physics, 2011, pp. 128–138.
[13] L.T. Dechevsky, P. Zanaty, A. Lakså, B. Bang, First instances of generalized expo-rational finite elements on triangulations, in: Applications of Mathematics and Engineering and Economics 2011, 1410, American Institute of Physics, 2011, pp. 49–61.
[14] G. Xu, G. Wang, AHT Bézier curves and NUAHT B-spline curves, J. Comput. Sci. Tech. 22 (4) (2007) 597–607.
[15] C. de Boor, A Practical Guide to Splines, Springer-Verlag, New York, 1978.
[16] G.I. Marchuk, V.I. Agoshkov, Introduction in Projective Grid Methods, Nauka, Moscow, 1981 (in Russian).
[17] A.R. Kristoffersen, L.T. Dechevsky, A. Lakså, B. Bang, Comparison between polynomial, Euler beta-function and expo-rational B-spline bases, AIP Conf. Proc. 1410 (1) (2011) 98–110, http://dx.doi.org/10.1063/1.3664360.
[18] D.W. Hahn, M.N. Özisik, Heat Conduction, third ed., John Wiley & Sons, Inc., Hoboken, New Jersey, 2012.
[19] E.H. Doha, A.H. Bhrawy, M.A. Saker, On generalized Jacobi-Bernstein basis transformation: Application of multi-degree reduction of Bézier curves and surfaces, J. Comput. Inf. Sci. Eng. 14 (2014) http://dx.doi.org/10.1115/1.4028633.
[20] O.C. Zienkiewicz, R.L. Taylor, J.Z. Zhu, The Finite Element Method: Its Basis and Fundamentals, sixth ed., Elsevier Butterworth-Heinemann, Linacre House, Jordan Hill, Oxford OX2 8DP, 2005.
[21] R. Dalmo, Local refinement of ERBS curves, in: V. Pasheva, G. Venkov (Eds.), in: 39th International Conference Applications of Mathematics and Engineering and Economics AMEE13, vol. 1570, AIP Publishing, 2013, pp. 204–211.